On the hydro-acoustic coupling responsible for the flashback limit-cycle of a premixed flame at a backward-facing step

Stéphane Boulal, Aurelien Genot, Jean-Michel Klein, Yves Fabignon, Axel Vincent-Randonnier, Vladimir Sabelnikov

On the hydro-acoustic coupling responsible for the flashback limit-cycle of a premixed flame at a backward-facing step

Stéphane Boulal[a,*], Aurelien Genot[a], Jean-Michel Klein[a], Yves Fabignon[a], Axel Vincent-Randonnier[b], Vladimir Sabelnikov[a]

[a] *DMPE, ONERA, Université Paris Saclay, F-91123, Palaiseau, France*
[b] *ONERA / DMPE, Université de Toulouse, F-31055, Toulouse, France*

Abstract

This paper examines the combustion dynamics of a methane/air premixed flame establishing past a backward-facing step placed in a ducted combustor. Spectral analysis performed on high-speed recordings of the flame allows to show that the flame dynamics is governed by two main components. The first one is an acoustic longitudinal resonance, which imposes a flapping motion of the flame around the step. The second one is a hydrodynamic instability, which corresponds to the roll-up of the flame by the recirculation region in the trail of the step. When the frequencies associated to each mechanism are far apart, the flame is relatively stable. When the two frequencies get closer, the roll-up process is amplified and leads to a more pronounced dilatation of the recirculation bubble, as well as an enhanced vertical flame flapping. When the two frequencies coincide, a fully-coupled hydro-acoustic instability is established and prompts the flame to periodically flashback in that it is favored by the fact that the fluctuations of the hydro-acoustically modulated flow velocity are so large that the flow velocity drops below the flame speed. Besides, an acoustic analysis of the ducted combustor reveals the presence of an acoustic velocity anti-node at the position of the step, which is exacerbating the amplitude of the fluctuations. Time series analyses of the flame position, reduced to a 1D description of its rotational motion, reveals that the flashback dynamics is locked to a limit-cycle attractor. The flashback motion is intermittently accompanied with the stochastic generation of an autoignition front developing from a hot spot located on the top wall.

Keywords: Combustion Instability, Flashback, Backward-Facing Step, Modal Analysis, Coherent structures, Limit-cycle

Novelty and Significance Statement

This work further analyses the high-speed recordings [1–4] of a premixed flame front establishing past a backward-facing step using a spectral analysis based on the rather recent SPOD technique [5]. The mechanism responsible for the flame flashback limit-cycle is clearly identified as resulting from *(i)* a hydro-acoustic coupling, and *(ii)* the large modulation of the flow velocity induced by the coupling such that the flame speed periodically overtakes the flow velocity. A kinematic model for the flame front position is proposed and is in good agreement with the observations. The work constitutes a case where the hydro-acoustic coupling is self-sufficient to explain the observed combustion instability. Finally, we complete the experimental observations of [1–4], whereby the stochastic generation of an autoignition front during some flashback cycles was missed.

Author Contributions

SB conceived the work and carried out the analyses. AG, AVR and VS initiated the framework for this study. SB, AG, JMK, and VS contributed to the interpretation of the results. YF performed the acoustic modeling. VS conducted the experiments. SB, AVR, and VS contributed to the data curation.

*Corresponding author: stephane.boulal@onera.fr

1. Introduction

Flame flashback is still a major concern for the design of combustion chambers [6, 7], for which the structural integrity may be compromised by the massive motion of the flame towards the injection, in possibly uncooled locations, as well as by pressure oscillations caused by the thermo-acoustic feedback.

Such a flame propagation is either caused by *(i)* a process of autoignition, whereby abnormally high temperatures of the fresh mixture could prompt the development of new reaction spots [8], or *(ii)* a process of convection-diffusion, whereby the flow velocity u falls below the flame propagation speed s_f [9]. The latter occasionally occurs in a great number of practical combustion devices, where a flame has to be stabilized in flows where u is greater than s_f [10]. Flame anchoring is indeed not achievable in uniform flows without the use of special geometries such as swirlers, bluff-bodies or Backward-Facing Steps (BFS) [11, 12]. These solutions create flow recirculation, which aims at creating local stagnation spots, *i.e.*, regions where $u \approx s_f$, thereby favoring the flame stabilization. However, one intrinsic drawback of implementing low-velocity stagnating regions is the increased propensity for flashback, through mechanisms like vortex breakdown [13], core flow flashback [6], or boundary layer flashback [14, 15]. Flashback is even more likely to occur in the presence of combustion instabilities [16], because the flame anchoring spot could follow velocity oscilla-

tions and in turn prompts the flame to propagate towards critical regions such as boundary layers [16–19]. In the worst case scenario where the reactants need to be premixed before reaching the combustor and no flame arrestors are installed upstream, the flashback can escalate into a detonation, resulting in even more catastrophic consequences. Moreover, with the current trend towards the use of hydrogen (H_2) or hydrogen-enriched fuel in gas-turbine combustors, the tendency for the flame to flashback may increase due to the fact that the speed of hydrogen-fueled flames is generally one order of magnitude higher than that of flames fueled by kerosene [20] or natural gas [21].

Many studies aimed at studying the structure, natural frequencies, and growth rates of both *(i)* acoustic and *(ii)* hydrodynamic modes, whose coupling could lead to flashback [22]. The first kind *(i)* relates to the onset of standing acoustic waves within a combustor. They depend on the geometry and boundary conditions, as well as on the sound speed a [23] and on the flow characteristics. Furthermore, the presence of heat release in the process could contribute to the amplification of the instability by the generation of sound in response to fluctuations of the Heat-Release-Rate (HRR) in a process commonly referred to as a thermo-acoustic coupling. The second kind *(ii)* relates to the evolution of vorticity in non-uniform flows [24]. This is, in particular, the case of shear or mixing layers, whereby coherent motions and quasi-periodic flow patterns such as the Kelvin-Helmholtz or the Benard-Von Karman instabilities are occurring [25, 26]. These phenomena are usually self-similar such that their characteristic frequencies f_h could be non-dimensionalized by means of a Strouhal number:

$$\mathrm{St} = \frac{f_h d}{u} \tag{1}$$

where u denotes the characteristic velocity of the problem (generally that of the bulk flow) and d is a characteristic length representative of the geometry responsible for the instability. In addition, the superimposition of a flame to these instabilities may alter the hydrodynamic modes through density gradients, which can generate (or annihilate) vorticity according to mechanisms such as dilatation or baroclinic torque [27, 28].

Furthermore, the presence of both acoustic and hydrodynamic modes can lead to additional couplings prone to trigger combustion instabilities. To this extent, Hemchandra *et. al.* [22] proposed two scenarios in which this could occur. First, if an hydrodynamic mode appears to be self-excited, it could trigger excitations at the frequency f_h regardless of the acoustic eigenfrequency f_a. The closer f_a and f_h get, the stronger the coupling with the acoustic mode is [26, 29, 30] (because perturbations at the frequency f_h become less evanescent), resulting in stronger HRR oscillations. Secondly, an hydrodynamic mode, which is globally stable but receptive to an excitation at the frequency f_a, could generate HRR oscillations, which - if a thermo-acoustic coupling is at play - could trigger additional acoustic velocity fluctuations, thus closing the loop with the excited hydrodynamic mode [22, 31].

One well known combustor geometry is the Backward-Facing Step (BFS), represented in Figure 1. The presence of the step dictates the formation of a shear-layer consecutive to

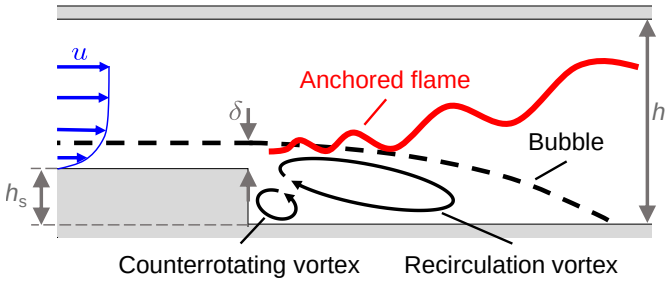

Figure 1: Main flow features of a flame stabilized behind a backward-facing step.

the detachment of the boundary-layer. The flow ultimately re-attaches some distance downstream enclosing a recirculation bubble, which contains a recirculation and a counterrotating vortex. In reacting conditions, the presence of recirculating hot gases is favoring the stabilization of the flame front, about the shear-layer. Various studies focused on the hydrodynamic instabilities (and associated Strouhal numbers) resulting from BFS geometries [32–35]. These are the Kelvin-Helmholtz instability [32, 36, 37], and the phenomena of vortex pairing [38], or shear-layer flapping [39–42]. Combustors equipped with BFS are indeed prone to all of the couplings discussed above. Depending on the operating conditions [43–45], the turbulence levels [46], and on the boundary conditions [3, 19], the flame could oscillate in various ways and at several frequencies. These oscillations root from the shear-layer unsteadiness, which is either self-excited or externally (acoustically) forced. The flame responds back by the generation of pressure fluctuations according to a process by which the ignition of rolled-up reactant pockets induces fluctuations of the flame surface area [11, 29, 30, 47]. In some cases, the shear-layer oscillations are so much amplified that the rolled-up reactants reach the bottom wall. As sketched in Figure 2, the roll-up actually occurs around the whole recirculation area, resulting in fresh gases trapped between the combustor wall and the recirculation bubble (a). These fresh gases then react leading to the overall dilatation of the bubble (b). In response, this entails the vortices and the flame front to ascent above the step (c). Such a scenario is favorable for the onset of the flashback [19, 43, 44, 48] since it implies that the flame front locally circumvents the tip of the step to reach the low-velocity region found in the boundary layer.

In short, unsteady motion of a flame anchored about a BFS could be caused by a self-excited (absolutely unstable) hydrodynamic mode [22, 28] combined or not to a thermo-acoustic coupling depending on whether the dilatation (HRR maximum) is in-phase with a pressure maximum imposed by the acoustic resonance [19, 44].

In this paper, we re-investigate results of experimental campaigns [1–4] conducted at the LAERTE facility of ONERA between the years 2004 and 2006. More specifically, we analyse the recordings of visible luminosity and OH* chemiluminescence of a premixed methane/air flame stabilized more or less steadily in a ducted combustor by means of a BFS. The coherent motions of the flame front are extracted by means

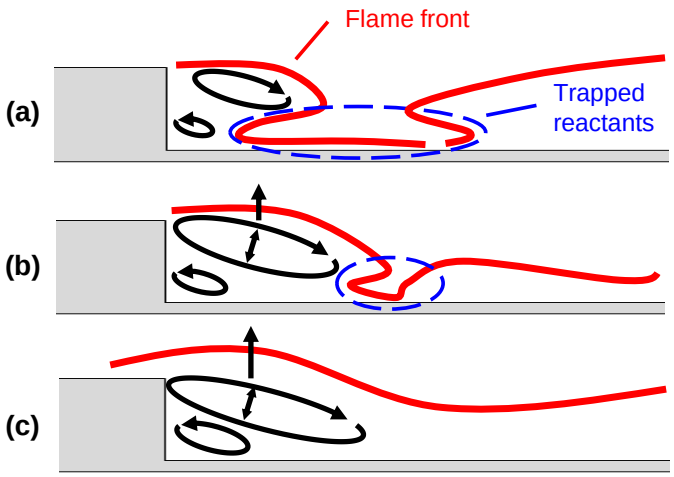

Figure 2: Schematic view of the flame roll-up and bubble dilatation mechanisms favoring the onset of a flashback. **(a)** trapped reactants, **(b)** burning of the fresh gas pocket leading to dilatation, **(c)** upward motion of the flame and tendency for it to flashback in the boundary layer.

of a modal analysis and are examined in light of the above-mentioned thermo-hydro-acoustic couplings. The conditions leading to the flashback limit-cycle are identified and put into perspective with those previously described in BFS combustors.

In Sect. 2, we briefly remind the experimental setup, the operating conditions of the cases of which the imaging results are provided in Sect. 3. In this section, an analytical acoustic model is also provided in order to help at the identification of the coherent motions constituent of the flame dynamics and extracted by means of a Spectral Proper Orthogonal Decomposition (SPOD) analysis conducted in Sect. 4. In particular, the hydro-acoustic coupling responsible for the flashback is described. In Sect. 5, we provide a quantitative argument explaining how the flashback emerges when the hydro-acoustically modulated velocity of the flow drops below the flame speed. In Sect. 6, the nature of the flashback limit-cycle is characterized.

2. Experimental setup

2.1. Backward-facing step ducted-combustor

Two versions of a ducted combustion chamber were used in the experiments. They are labeled Cfg. A and Cfg. B. Both setups consist of a tunnelled combustion chamber equipped with a backward-facing step at about its mid-section. This simple design was thought as a mean for the study of the mechanisms of flame stabilization behind obstacles, with applications ranging from afterburners to ramjets. Both setups are sketched in Figure 3. The combustion chamber has a 100×100-mm^2-square cross-section. The step height is $h_s = 35$ mm. At the front-end, preheated air of mass flow-rate $\dot{m}_{air}$ is delivered to the combustion chamber by means of a choked nozzle. The main difference between the two configurations resides in their inlet geometries **(1a or 1b)** and on their acoustic properties. The shape of the throttling plug **(8)** also sligthly changes from one configuration to the other.

For the Cfg. A, a nozzle is located much upstream of the combustor (not represented in Fig. 3). Downstream of the nozzle, the choked air flows through an intake manifold (a plenum), whereby it is distributed towards four inlets connected to the ducted combustor **(1a)**. Then, the air passes through a 100-mm-long honeycomb grid (triangular pattern of $\Delta = 10$-mm-pitch size) **(2a)**. The purpose of the grid is to straighten the turning flow created by the 90° injection and to soften the turbulence intensity generated by the impingement of the four intakes.

For the Cfg. B, which was implemented after the Cfg. A, the complex flow pattern was simplified, in that the inlet nozzle **(1b)** was moved much closer to the combustion chamber. The choked flow imposes the creation of a shock train along which the flow transits from supersonic to subsonic conditions. This phenomenon has ill-understood acoustic properties. Culick and Rogers [49, 50] proposed to model it as a normal shock. To a first-order approximation, this shock could be treated as a closed acoustic boundary condition.

Methane (CH_4) of mass flow-rate $\dot{m}_{CH4}$ at the ambient temperature is injected through 55 regularly spaced holes drilled in five vertical manifolds **(3)**. The then formed methane/air mixture passes through a 100-mm-long honeycomb grid **(4)** (triangular pattern of $\Delta = 5$-mm-pitch size) whose purpose is to homogenize the flow velocity profile and the mixture composition, while decreasing the turbulence level. After the flow passes by the honeycomb grid, its composition can reasonably be considered as uniform with an equivalence ratio $\phi = (\dot{m}_{air}/\dot{m}_{CH4})_{st.}/(\dot{m}_{air}/\dot{m}_{CH4})$, where $(\dot{m}_{air}/\dot{m}_{CH4})_{st.} = 17.3$ is the stoichiometric air-to-fuel ratio. Downstream of the BFS **(5)**, a spark-igniter **(6)** is flush-mounted to the bottom wall surface. In nominal operation, once ignited, the flame front stabilizes about the position of the step because of the recirculation zone formed on its trail and thanks to the low-velocity regions thereby created. The inlet temperature of the airflow T_0 can be controlled up to a limit of 650 K, which is much lower than the $\sim 800-900$ K autoignition temperature of methane/air mixtures [51]. At the back-end of the combustor, a converging nozzle completes the system **(8)**. The surface area of its throat can be adjusted by means of a throttling plug travelling horizontally. As such, the chamber pressure P can be controlled. An indirect consequence of throttling the plug is to alter the back-end acoustic impedance. The pressure oscillations were monitored by means of two dynamics pressure transducers mounted on the top-wall. Their recordings and analyses are provided in [1–4].

At about the position of the step, two 260-mm-long, 100-mm-high fused silica windows **(7)** are placed providing lateral visualization accesses. The combustion chamber walls are water-cooled except around the locations of the visualization windows. Throughout the different experimental campaigns, a variety of optical diagnoses were implemented: Particle Image Velocimetry (PIV) [2–4], Planar Laser Induced Fluorescence of the OH radicals (PLIF-OH) imaging [1–4], visible luminosity imaging [1], CH* chemiluminescence imaging [1] and OH* chemiluminescence imaging [1–4]. For the PIV and PLIF-OH measurement techniques, a third optical access is mounted on the top walls for the purpose of generating laser sheets. In the

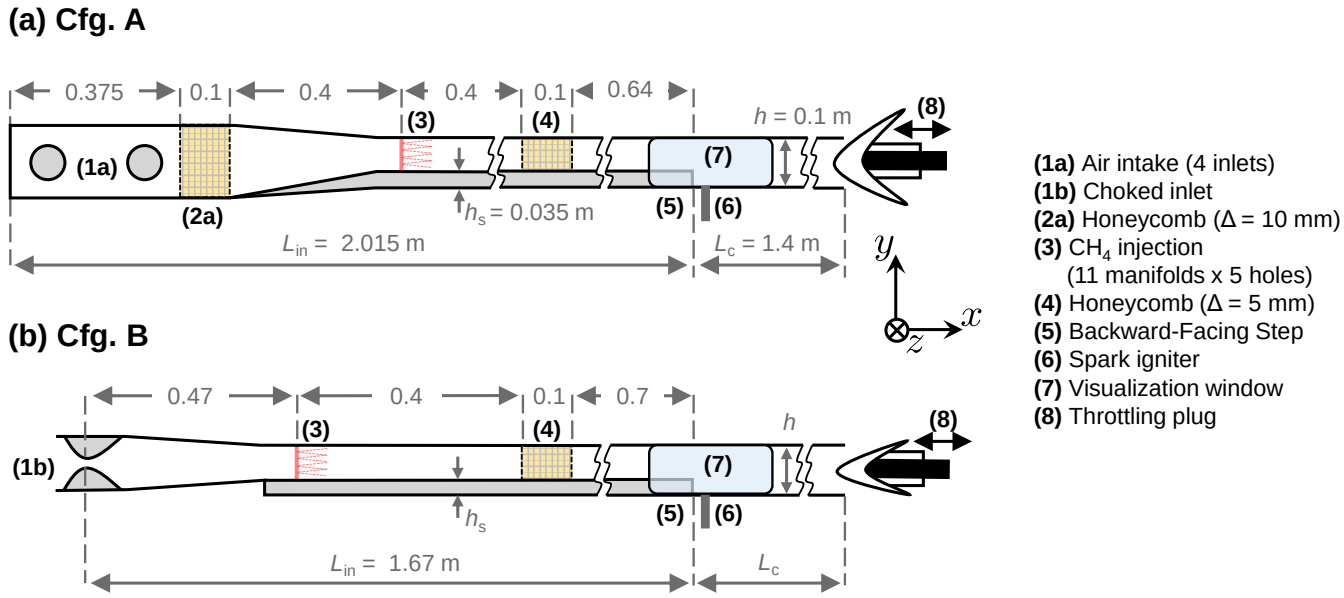

Figure 3: Schematic views of the backward-facing step ducted-combustor in the Cfg. A **(a)** and Cfg. B **(b)**. The horizontal lengths are not to scale and specified in meter.

following, we re-examine the flame recordings obtained with high-speed acquisition rates, *i.e.*, the flame visible luminosity recordings of [1] acquired with a 1-kHz-rate and the OH* chemiluminescence recordings of [1–4] acquired with a 4-kHz-rate. Details of the visualization techniques as well as equipments used at the time can be found in the above-mentioned references.

2.2. Operating conditions

We focus our analysis on three cases, for which the flame exhibited three distinct behaviors: a stable behaviour (Stable Case), a near-stable behaviour (Metastable Case) and an unstable behaviour, that of a periodic flame flashback (Unstable Case). The later has already been described in [1–4], whereas the Stable and Metastable cases were not. These two were obtained in Cfg. A, while the Unstable Case was observed in Cfg. B. For each case, Table 1 lists the operating conditions achieved in terms of the chamber pressure P, the inlet air temperature T_0, the air mass flow-rate $\dot{m}_{\text{air}}$ and of the equivalence ratio ϕ of the ideal methane/air mixture. Table 1 also provides with the cross-sectional average inlet velocity u_0, *i.e.*, that before the step. The inlet flow is characterized by a Reynolds number (based on the duct heigth $h - h_s$) of 1.2×10^5, which is one to two order(s) of magnitude larger than those reported in similar works related to flame instabilities in combustors equipped with BFS [44, 45, 52, 53]. As such, the proposed work is more representative of industrial applications such as ramjets or thrust augmentors. In [2–4], the rms of the velocity fluctuations upstream of the step (Stable Case) was measured to $u_{\text{rms}} \approx 10$ m/s by means of a PIV setup. For now, let us suppose that theses fluctuations are only of turbulent, *i.e.*, stochastic nature. For the equivalence ratio and mixture temperature considered in this work (Tab. 1), the laminar flame speed is evaluated to $s_{\text{L}} \approx 0.5$ m/s for the Stable and Metastable cases,

Case	Stable	Metastable	Unstable
Cfg.	A	A	B
$\boldsymbol{P}$ **(bar)**	1.05	1.44	1.35
$\boldsymbol{T_0}$ **(K)**	460	460	550
$\boldsymbol{\dot{m}_{\text{air}}}$ **(kg/s)**	0.28	0.28	0.27
$\boldsymbol{\phi}$	0.82	0.82	0.82
$\boldsymbol{u_0}$ **(m/s)**	59	44	51
$\boldsymbol{M_0}$	0.14	0.10	0.11

Table 1: Experimental conditions (averaged values) of the cases reported, $\boldsymbol{P}$: combustor pressure, $\boldsymbol{T_0}$: inlet air temperature, $\boldsymbol{\dot{m}_{\text{air}}}$: air mass flow-rate, $\boldsymbol{\phi}$: methane/air mixture equivalence ratio, $\boldsymbol{u_0}$: inlet velocity, $\boldsymbol{M_0}$: inlet Mach number.

and $s_{\text{L}} \approx 0.8$ m/s for the Unstable Case [54]. Hence, the ratio u'/s_{L} is framed such that $10 \lesssim u'/s_{\text{L}} \lesssim 20$. The turbulence integral length scale is estimated using the correlation for fully developed pipe flow: $\ell_{\text{t}} = 0.038 d_{\text{h}}$, with d_{h} the hydraulic diameter of the combustor upstream of the step, *i.e.*, $d_{\text{h}} = 79$ mm. This yields $\ell_{\text{t}} \approx 3$ mm. At this point, it should be emphasized that the integral length scale could also depend on the honeycomb **(4)**, whose triangular cells admit an hydraulic diameter of 3.33 mm, very close to the value deduced from the correlation. As for the flame thickness, δ_ℓ^0, it is estimated from $\delta_\ell^0 = D_{\text{th.}}/s_{\text{L}}$, where $D_{\text{th.}}$ is the thermal diffusivity of the mixture (mostly composed of air). The value of δ_ℓ^0 is hence framed to within $80 \lesssim \delta_\ell^0 \lesssim 100$ µm, which yields $30 \lesssim \ell_{\text{t}}/\delta_\ell^0 \lesssim 40$. Consequently, the combustion is supposed to occur in the thickened flames (thin reaction zones) regime according to the classification of turbulent combustion regimes proposed by Borghi [55]. More precisely, this corresponds to the following ranges of turbulent Reynolds, Dahmköhler, and Karlovitz numbers: $\text{Re}_{\text{t}} = u'(h - h_{\text{s}})/\nu_{\text{air}} \in [1.1 \times 10^3, 1.3 \times 10^3]$ (ν_{air} is the air kinematic viscosity), $\text{Da}_{\text{t}} = (\ell_{\text{t}}/\delta_\ell^0)/(u'/s_{\text{L}}) \in [1.5, 4]$ and

$\mathrm{Ka} = \sqrt{\mathrm{Re_t}}/\mathrm{Da_t} \in [8, 24]$. Therefore, it is assumed that the flame dynamics is dominated by three components: thickening, wrinkling and motions.

2.3. Preliminary acoustic characterization

Before presenting and analysing the results, we propose to first determine the acoustic eigenfrequencies of the geometry. If we neglect, in a first approach, the potential effects induced by the inlet shock train (for Cfg. B), the upstream converging section, the honeycomb grid(s) and the fuel manifolds, the upstream boundary condition is assumed to be that of a rigid wall. The critical pressure of the flow is $P_{\mathrm{crit.}} = (2/(\gamma+1))^{\gamma/(1-\gamma)} P_{\mathrm{atm.}}$, where $P_{\mathrm{atm.}}$ is the atmospheric pressure. Thus, for a stream of heat capacity ratio γ framed such that $1.2 < \gamma < 1.4$, it follows that $1.8 < P_{\mathrm{crit.}} < 1.9$ bar. Therefore, for the combustor pressure considered here (see Tab. 1): $P < P_{\mathrm{crit.}}$, which implies that the flow is not choked in the duct. Thus, from the acoustic viewpoint, the constricted area formed by the throttling plug at the back end of the combustor is not equivalent to a rigid wall reflecting the sound waves. For both configurations, Figure 4 schematically shows the simplified acoustic configuration by which the combustor is modeled. It consists of two connected cavities (labeled "0" and

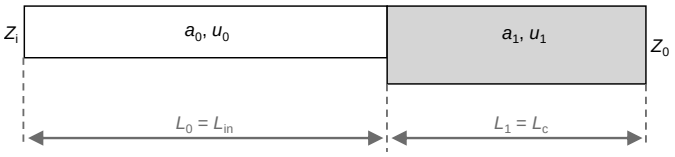

Figure 4: Schematic view of the acoustic model of the ducted combustors.

"1") of uniform physical properties separated by an interface which represents the flame front. These cavities are characterized by their lengths $L_0 = L_{\mathrm{in}}$ and $L_1 = L_{\mathrm{c}}$, and cross-sections $S_0 = h(h - h_{\mathrm{s}})$ and $S_1 = h^2$ (see Fig. 3 for reference). The inlet and outlet impedances are labeled Z_{i} and Z_{o}, respectively. The first cavity ("0") is filled with unburnt gases of which the sound speed is $a = a_0$, which writes $a_0 = \sqrt{\gamma_0 R/W_0 T_0}$, with $R = 8.314$ J/mol/K the universal gas constant and W_0 the molecular weight of the gas. In a first approach, we consider that the unburnt gas are only composed of air at the temperature T_0, *i.e.*, the mixing with the colder methane is not considered: $\gamma_0 = \gamma_{\mathrm{air}} = 1.4$ and $W_0 = W_{\mathrm{air}} = 29$ g/mol. As for the second cavity ("1"), we consider that it is filled with combustion products of which the properties, γ_1, W_1, T_1 and $a_1 = \sqrt{\gamma_1 R/W_1 T_1}$ are evaluated by means of the NASA-CEA thermochemical code. The values for T_1 and a_1 are absolute upper limits, considering that the combustion is, with certainty, not perfect. The velocity u_1 of the flow in the burnt gases is evaluated owing to the mass conservation: $u_1 = (\rho_0/\rho_1)(1 - h_s/h)u_0$. Note that this approach neglects the active flame effects on the acoustic. Table 2 compiles the values used for the evaluation of the eigenfrequencies proposed in the following.

In the ideal case with a sufficiently small cross dimension, *i.e.*, $h \ll L_1 + L_2$, we consider that the acoustic pressure and velocity perturbations, $\widetilde{p}$ and $\widetilde{u}$, are the same over the cross-section. That is the wave front is treated as a plane normal to

Case	Stable	Metastable	Unstable
Cfg.	**A**	**A**	**B**
L_0 **(m)**	2.015	2.015	1.67
L_1 **(m)**	1.4	1.4	1.4
S_0 **(m^2)**	6.5×10^{-3}	6.5×10^{-3}	6.5×10^{-3}
S_1 **(m^2)**	1.0×10^{-2}	1.0×10^{-2}	1.0×10^{-2}
a_0 **(m/s)**	430	430	470
a_1 **(m/s)**	880	881	889
u_0 **(m/s)**	59	44	51
u_1 **(m/s)**	182	136	135

Table 2: Physical properties considered for the low-order acoustic modeling of the ducted combustor.

the longitudinal direction. In the framework of the linear acoustic theory of an inviscid stationary medium (labeled m), the one dimensional homogeneous partial differential equation for the pressure fluctuations writes:

$$\frac{\partial^2 \widetilde{p}}{\partial t^2} + 2u_m \frac{\partial^2 \widetilde{p}}{\partial t \partial x} + (u_m^2 - a_m^2)\frac{\partial^2 \widetilde{p}}{\partial x^2} = 0 \tag{2}$$

In the frequency space, the general solution is:

$$\begin{cases} \widehat{p}(x,f) = e^{jMk_{\mathrm{c},m}x}\left(A_{\mathrm{I}}e^{-jk_{\mathrm{c},m}x} + A_{\mathrm{R}}e^{jk_{\mathrm{c},m}x}\right) \\ \widehat{q}(x,f) = \dfrac{e^{jMk_{\mathrm{c},m}x}}{Y_m}\left(A_{\mathrm{I}}e^{-jk_{\mathrm{c},m}x} - A_{\mathrm{R}}e^{jk_{\mathrm{c},m}x}\right) \\ \text{with } k_{\mathrm{c},m} = \dfrac{k_m}{1-M_m^2} \text{ and } k_m = \dfrac{2\pi f}{a_m} \end{cases} \tag{3}$$

where $\widehat{\cdot}$ denotes the Fourier transform of a given quantity, $\widehat{q} = \rho_m S_m \widehat{u}$ is the acoustic mass flow rate, k is the wave number, $M_m = u_m/a_m$ is the Mach number, $Y_m = a_m/S_m$ is an acoustic characteristic of the medium, and A_{I} and A_{R} are two constants associated to the incident and reflected waves, respectively. Meissner [56] derived a simple analytical method to estimate the eigenfrequencies of longitudinal modes in ducts with discontinuities based on a general expression of the acoustic impedance $Z = \widehat{p}/\widehat{q}$. We extend this method to account for the differences of sound speed and flow velocity across the interface separating the two cavities. The eigenfrequencies could be computed by cancelling the following G-function, *i.e.* a dispersion relation, of which f is the unknown. Formally, this writes:

$$\mathrm{G}(f) = Y_0 - Y_1 \tan\left(k_{\mathrm{c},1}L_1\right)\tan\left(k_{\mathrm{c},0}L_0\right) = 0 \tag{4}$$

This equation assumes a rigid wall at the inlet ($Z_{\mathrm{i}} = \infty$) and an open boundary at the outlet ($Z_{\mathrm{o}} = 0$). In the case of rigid walls placed at both extremities ($Z_{\mathrm{i}} = Z_{\mathrm{o}} = \infty$), the G-function is slightly different:

$$\mathrm{G}(f) = Y_0 \tan\left(k_{\mathrm{c},1}L_1\right) + Y_1 \tan\left(k_{\mathrm{c},0}L_0\right) = 0 \tag{5}$$

Since the outlet acoustic impedance Z_{o} is unknown, we can only, at this stage, frame the value of the expected eigenfrequencies between the two limiting models of a closed/open tube (Eq.(4), *i.e.*, a quarter-wave resonance, and a closed/closed tube (Eq.(5), *i.e.*, a half-wave resonance. Table 3 provides with

Case	Stable	Metastable	Unstable
Cfg.	**A**	**A**	**B**
Closed-open tube			
f_{1L} **(Hz)**	35	36	44
f_{2L} **(Hz)**	113	115	143
Closed-closed tube			
f_{1L} **(Hz)**	80	81	99
f_{2L} **(Hz)**	152	155	187

Table 3: Framing of the eigenfrequencies f_{1L} and f_{2L} for the three cases between the limiting acoustic models of the closed-open tube (quarter-wave resonance) and the closed-closed tube (half-wave resonance).

the values of the eigenfrequencies (fundamental and first harmonic) returned in both configurations and for the three cases considered. As mentioned above, the flow is not choked at the outlet of the combustion chamber. Thus, from the acoustic viewpoint, the measured acoustic eigenfrequencies, should be closer to the values calculated with the closed/open approximation. For the closed/closed configuration, we observe that the frequency f_{2L} is not exactly twice the frequency f_{1L}, as it would have been expected for a pure half-wave resonator. Similarly, for the closed/open configuration, f_{2L} is not exactly $3f_{1L}$, as it would have been expected for a pure quarter-wave resonator. This is explained by the fact that the physical properties as well as the cross-sectional area jump from one cavity to the other.

The overestimation of the sound speed in the burnt gases (domain "1") is of second order importance in the evaluation of the eigenfrequencies. For example, a 10% overestimation of burnt gases temperature would only induce a 5% overestimation of the sound speed in the domain since $a_1 \propto \sqrt{T_1}$, which in turn only overestimate the frequencies f_{1L} according to:

$$\frac{\Delta f_{1L}}{f_{1L}} \approx 1 + \frac{L_1}{L_0 + L_1}\frac{\Delta a_1}{a_1} \approx 1 + \frac{L_1}{2(L_0 + L_1)}\frac{\Delta T_1}{T_1} \approx 1.02 \quad (6)$$

, that is a 2% overestimation. Here, we have neglected the reduction of the flow velocity u_1 because its influence is of second order (the term $1 - M_1^2$ in Eq.(3)) in the evaluation of the eigenfrequencies.

As for the transverse eigenmodes in the direction y and z, the frequencies of the fundamental modes could be framed such that $3310 < f_{1T_y} < 3620$ Hz and $2150 < f_{1T_z} < 2350$ Hz in the first cavity (upstream of the step) and $4400 < f_{1T_y} = f_{1T_z} < 4445$ Hz in the second cavity (downstream of the step).

3. Results

In this section, we provide a qualitative description of the flame dynamics obtained in the three different cases. Figure 5 shows instantaneous snapshots of the recordings associated to each case (visible luminosity imaging for the Stable and Metastable cases and OH* chemiluminescence imaging for the Unstable Case). In order to better appreciate the different dynamics returned by each case, we refer the readers to the videos included in the Supplementary materials S1, S2 and S3. Figure 6 provides with the mean and Root Mean Square (RMS) fields computed over the recording periods. For the Stable and Metastable cases, the mean position of the flame front is indicated by a red-dotted line. This will be used in the quantitative argument of Sect. 5.

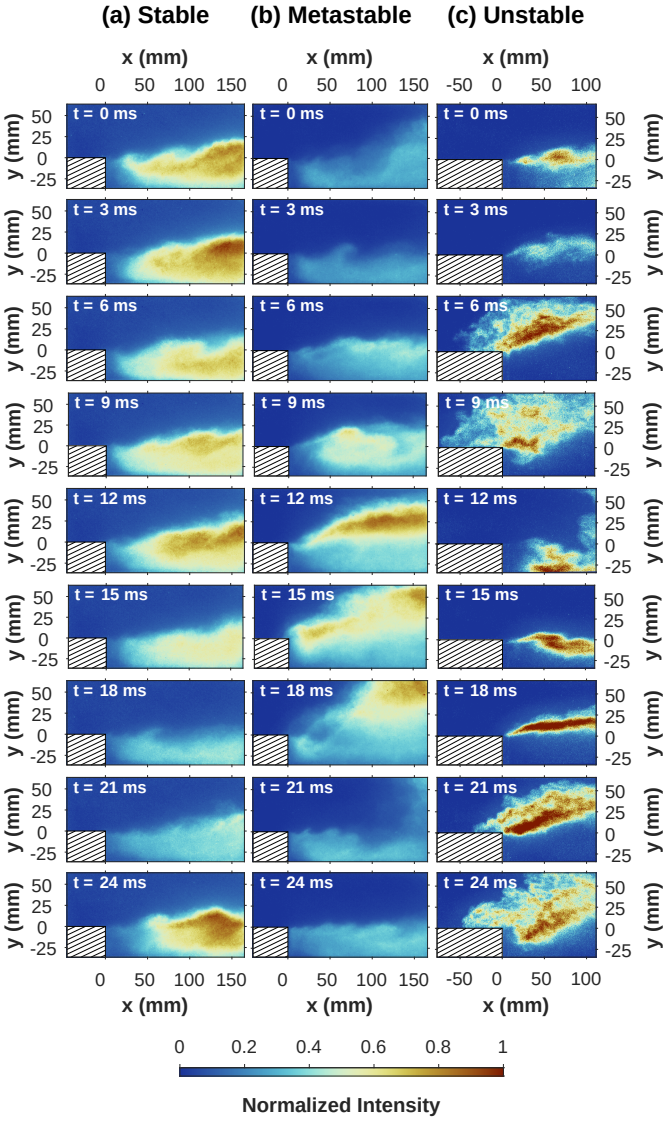

Figure 5: Fluctuations of the normalized flame intensity captured by means of visible luminosity **(a, b)** or OH* chemiluminescence **(c)** high-speed imagings for the Stable **(a)**, Metastable **(b)** and Unstable **(c)** cases. The time-step between each frame is 3 ms. The dashed box on the bottom left corner represents the backward-facing step. Videos showing each case dynamics are provided in the Supplementary materials S1, S2 and S3.

For the Stable Case (Fig. 5(a)), we observe that the flame is anchored in the vicinity of the step and that it moves about its mean position according to an up-and-down flapping motion. Qualitatively, the flame motion of the Stable Case is a composite between the *stable* and *buzzing* cases reported by Keller *et al.* [52]. The interface delineating the burnt gases from the fresh gases, *i.e.*, the flame front, is wrinkled by shedded vortices (a characteristic trait of the *stable* case) as a result of the density and velocity gradients across the shear layer (commonly referred to as Kelvin-Helmholtz instability [33]).

This is quite observable on the time frame $t = 0$ ms of Fig. 5(a). The flame wrinkling also combines with some vertical flapping motion (a characteristic trait of the *buzzing* case).

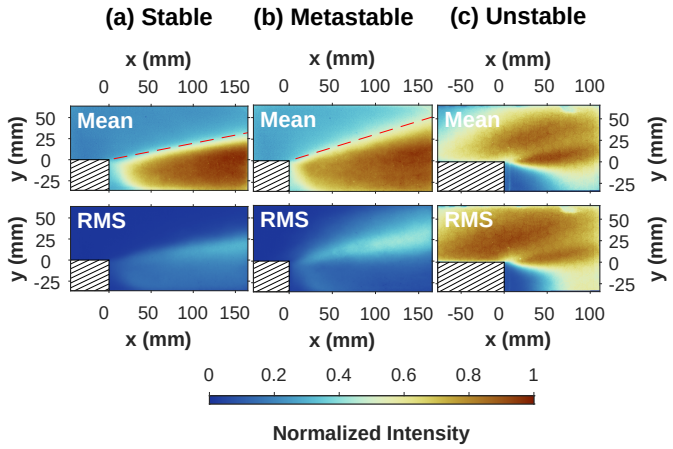

Figure 6: Normalized Mean and Root Mean Square (RMS) fields for the Stable **(a)**, Metastable **(b)** and Unstable **(c)** cases. The dashed box on the bottom left corner represents the backward-facing step. The red-dotted line represents the mean position of the flame front.

For the Metastable Case (Fig. 5(b)), the flapping motion of the flame is already much pronounced. This is clearly observable on the mean and RMS fields shown in Figure 6(b), whereby it is inferred that the spatial extent of the flame has progressed upward. Between $t = 12$ and $t = 15$ ms, we even observe that the flame circumvents the step tip in the upstream direction. This event could be viewed as a gentle flashback. Qualitatively, the flame motion of the Metastable Case is similar to the *buzzing* case reported in [52].

For the Unstable Case (Fig. 5(c)), the upstream incursion of the flame is here massive. However its amplitude is not constant (see the related video in the Supplementary material S3). It sometimes extend much upstream of the visualizations window. Qualitatively, the Unstable Case is similar to the *chucking* case reported by Keller *et al.* [52]. Note that the vertical flapping motion, although, here being much more massive, is somewhat similar to the flapping observed on the Stable and Metastable cases. One should also note that other studies, such as those of Altay *et. al.* [44, 53] or Hong *et. al* [45], reported experiments similar to those presented above and observed that the flashback was associated with the flame roll-up mechanism described in Sect. 1 (see Fig. 2). This roll-up mechanism also seems to be present in our experiments, *e.g.*, at $t = 12$ ms for the Unstable Case, or at $t = 18$ ms for the Metastable Case. Eventually, it should be emphasized that the ascent of the recirculation vortex, following the flame roll-up may also be linked to the vertical flapping motions described in both the present study and that of Keller *et al.* [52].

The next section provides with a modal analysis which aims at decomposing the flame motions, which, for now, has only be described on the surface. As it will be demonstrated in §4.3, the flashback motion reported in the present paper results from a coupling between the first longitudinal acoustic mode of the duct, which imposes a vertical flapping motion of the flame, and the hydrodynamic instability, that of the flame roll-up, developing in the trail of the step. The coupling induces massive velocity fluctuations up to the point that during the phase of decreasing velocity, the flow velocity at the step position drops below that of the flame, triggering the flashback event. This point will be quantitatively discussed in Sect. 5.

4. Spectral analysis

In this section, we further examine the dynamics qualitatively described above. To do so, we perform analyses based on the Spectral Proper Orthogonal Decomposition (SPOD) technique, whereby the flame motion is decomposed into coherent orthogonal modes (both in space and time) in an attempt to highlight the governing mechanisms responsible for the flame motion. The SPOD technique, in the form derived by Towne *et al.* [5], is a rather recent modal decomposition technique, which aims at extracting coherent mechanisms contained in a flow. We do not describe here the algebraic details of the technique. Thorough descriptions of modal decomposition methods applied to various fluid dynamics problems and comparisons between techniques could otherwise be found in [5, 57]. In [58], we have successfully applied the method to the case of a subscale rocket combustor and managed to spectrally characterize a combustion instability occurring within the combustor. We use again the same Matlab implementation (`spod`) of the algorithm [59]. Because of the memory limitation of the cameras used for the recordings, we choose to guarantee the most refined frequency resolution δf. As such, we set the number of blocks to its minimum, *i.e.*, $N_{\text{blck}} = 2$, with a 50-percent-overlap. The resulting frequency resolution is then $\delta f \approx 1.5$ Hz for the Stable and Metastable cases (visible luminosity imaging composed of $N_t = 1018$ snapshots recorded at a $f_s = 1$ kHz-acquisition rate) and $\delta f \approx 0.5$ Hz for the Unstable Case (OH* chemiluminescence imaging composed of $N_t = 12282$ snapshots recorded at a $f_s = 4$ kHz-acquisition rate). According to Nyquist theory, the spectral content achievable by the method reaches $f_s/2 = 0.5$ kHz for the visible luminosity imaging and $f_s/2 = 2$ kHz for the OH* chemiluminescence imaging. Although the recordings shown in Fig. 5 do not suggest that the transverse acoustic modes are excited, the limitations impaired by the quite low acquisition rates would have excluded the modes from being captured by the SPOD technique: $f_{1T} > f_s/2$.

4.1. Stable Case

Figure 7(a) shows the spectral density distribution computed by the SPOD for the Stable Case. Two peaks of small amplitudes emerge from the background: one at $f = 45$ Hz and the other one at $f = 73$ Hz. The shapes computed for these two modes are shown in Fig. 7(b) and (c), respectively. The shape of the first mode (Fig. 7(b)), at the frequency $f = 45$ Hz, suggests the vertical flapping of the flame front, which also recalls the flapping instability of the flame anchored at the lip of a coaxial rocket injector described in [58]. Its frequency lies well in-between the two limiting values determined in

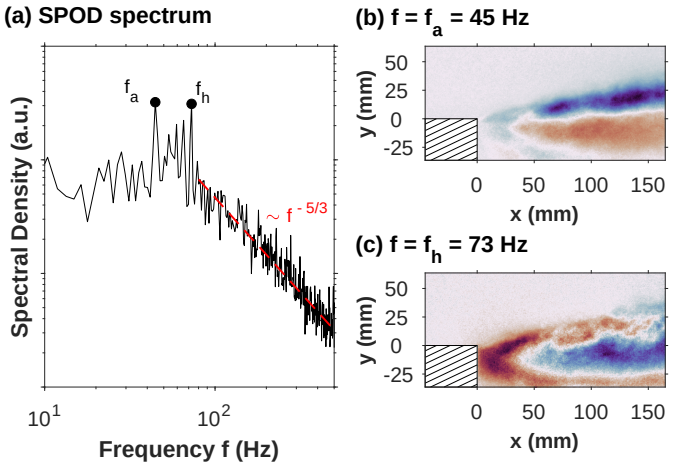

Figure 7: **(a)** SPOD spectrum of the recordings for the Stable Case. **(b)** SPOD shape of the $f = 45$-Hz mode. **(c)** SPOD shape of the $f = 73$-Hz mode. For each mode, an animation of the shape is provided in the Supplementary materials S4 and S5.

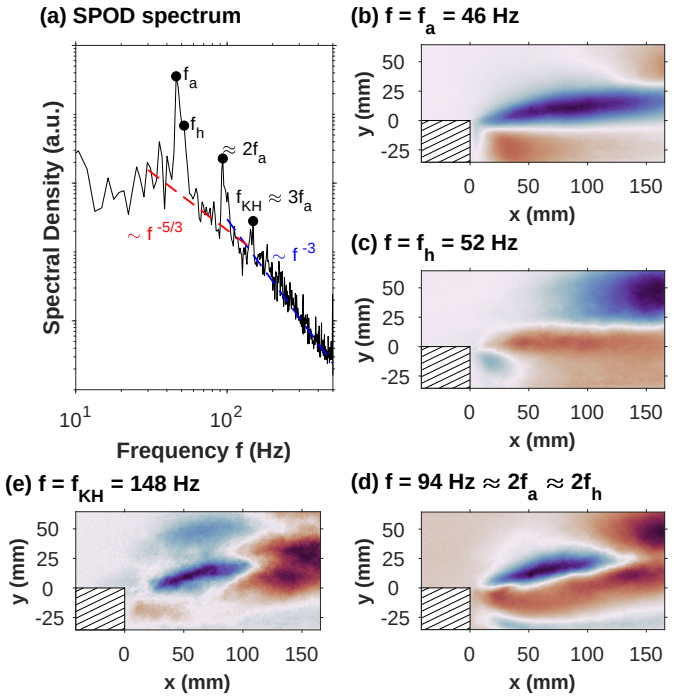

Figure 8: **(a)** SPOD spectrum of the recordings for the Metastable Case. **(b)** SPOD shape of the $f = 46$-Hz mode. **(c)** SPOD shape of the $f = 52$-Hz mode. **(d)** SPOD shape of the $f = 94$-Hz mode. **(e)** SPOD shape of the $f = 148$-Hz mode. For each mode, an animation of the shape is provided in the Supplementary materials S6 through S9.

the preliminary acoustic characterization of §2.3 (see also Table 3): $35 < f < 80$ Hz, more so to the model of a closed-open tube associated to a quarter-wave resonance. This gives us reasons to associate the flapping motion to an acoustic resonance of the ducted combustor. The frequency of this mode is henceforth referred to as f_a. Phenomenologically, we can understand it as coming from the interaction of the flame with a standing acoustic wave.The flame responds to the perturbation of the flow velocity induced by the wave by adjusting its position according to a rotational motion (the flapping) around the flame anchoring point, located in the vicinity of the step corner. This point will be quantitatively examined in Sect. 5.

The shape of the second mode (Fig. 7(c)), at the frequency $f = 73$ Hz, suggests the flame roll-up in the recirculation bubble combined with a wrinkling of the flame front. It corresponds to a hydrodynamic instability, thereby justifying the notation f_h. We characterize this instability by means of a Strouhal number St_h based on the step height h_s, and the bulk flow velocity u_0. We obtain a value $\mathrm{St}_h = f_h h_s / u_0 = 0.0433$.

4.2. *Metastable Case*

Figure 8(a) shows the spectral density distribution returned by the SPOD for the Metastable Case. Here, we observed four peaks of higher amplitudes standing out from the background: the first one at $f = 46$ Hz, the second one at $f = 52$ Hz, the third one at $f = 94$ Hz and the last one at $f = 148$ Hz. The shapes computed for these four modes are shown in Fig. 8(b), (c), (d) and (e), respectively. At higher frequencies, the spectrum follows a power law with an exponent -3. It would seem plausible to relate this to the inertial range observed in two-dimensional turbulence [60], for which the vorticity flow occurs at small scales. As opposed to this, for the Stable Case (see Fig. 7), the turbulence is three-dimensional (including in the shear layer). As such, the spectrum follows the classical $-5/3$ power law proposed by Kolmogorov for the turbulent energy spectra [61].

Qualitatively, the mode at the frequency $f = 46$ Hz (Fig. 8(b)) resembles to the mode linked to the acoustic resonance obtained for the Stable Case. Again, its frequency is well framed by the two limiting values determined in §2.3 (see also Table 3): $36 < f < 81$ Hz. Hence, we can reasonably presume that it is that of the longitudinal acoustic resonance. As a matter of fact, the sound speed is almost the same between the Stable and the Metastable cases (see Table 2). Therefore, there is no particular reason - if we neglect the flame response - for the combustor natural frequencies to change from one case to the other.

In contrast, the velocity u_0 significantly changes between the two cases (see also Table 2). As such, the mode at frequency $f = 52$ Hz (Fig. 8(c)) is associated to a Strouhal number $\mathrm{St}_h = 0.0414$, a value within 5% of the one evaluated for the Stable Case. This confirms the self-similar nature of the identified hydrodynamic instability.

The proximity between the two frequencies ($\Delta f = |f_a - f_h| = 6$ Hz) explains the broadening of the spectrum on the right side of the peak at $f = f_a$, and results from the coupling between the flame flapping due to both the acoustic resonance and the roll-up associated to the hydrodynamic instability. This phenomenon is well documented and identified as resulting from the coexistence between an absolutely unstable hydrodynamic mode and an acoustic mode [26]. The coupling is responsible for the overall higher amplitude observed on the frequency domain and for the larger amplitude of motion observed in the time domain. It also appears that

this mode has switched to a counter-clockwise rotation (see the Supplementary material S7). In fact, this mode shape now recalls the unsteady motion of the flame sketched in Fig. 2, and gives an even more clear interpretation of the process by which the hydro-acoustic coupling is amplified as Δf decreases: the vertical flapping "pushes" fresh gases toward the bottom wall, and the closer its frequency gets to that of the roll-up motion, the greater the amount of trapped gases. This mechanism tends to amplify the flapping motion, of which the signature is now also discernible on the shape of the mode at $f = f_h$.

The mode at the frequency $f = 94$ Hz (Fig. 8(d)) falls in between $2f_a = 92$ Hz and $2f_h = 104$ Hz. The shape is clearly resulting from the hydro-acoustic coupling. The spectrum broadening associated to the coupling is again observed. The entanglement of the shapes associated to the acoustic and hydrodynamic motions can also be noted (better appreciated on the animation of the Supplementary material S8). It is interesting to note that the presence of a peak at $2f_a$ is not expected: considering the combustor as a closed-open tube, only odd multiples of the fundamental frequency are supposed to get excited. Hence, the first harmonic should be found at $f_{2L} = 3f_{1L}$. For example, this was observed in [58] for which a quarter-wave resonance was observed in the oxygen feed line of the combustor. The excitation of both even and odd harmonics is a typical signature of a non-linear behaviour.

Finally, the mode at $f = 148$ Hz (Fig. 8(e)) is clearly that of a Kelvin-Helmholtz type instability, which seems to contain most of the flame wrinkling. The distinctive wave-packet structure returned by the SPOD is consistent with those observed in previous works, *e.g.*, [5, 58]. As a matter of fact the Strouhal number associated to the frequency $f = f_{KH} = 148$ Hz is $St_{KH} = 0.118$, a value in-line with those usually reported in the literature for this well-known "step mode" [32–35]. The frequency also falls between $3f_a$ and $3f_h$, which explains why this mode stands out from the background. This Kelvin-Helmholtz instability produces quasi-2D vertical structure followed by stochasticization and vorticity cascade to smaller scales (larger frequencies). This explains *a posteriori* the -3 power law trend obtained for $f \gtrsim f_{KH}$.

4.3. Unstable Case

Figure 9(a) shows the spectral density distribution computed by the SPOD for the Unstable Case. Here, we distinguish as much as six frequency peaks. They are all multiple of a fundamental frequency located at $f = 67$ Hz. The peaks are even more pronounced than in the previous cases. Qualitatively, this corresponds to the higher amplitudes of the flame motion reported for this case. The shapes computed for the two first modes are shown in Fig. 8(b) and (c). At higher frequencies, the spectrum is here closer to the $-5/3$ power law, because the heat release zone, *i.e.*, the flame front, moves as a whole with the 3D turbulence contained within it. Since the combustor acoustic properties, *e.g.*, the sound speeds and the lengths, differ from those of the two previous cases, there is no reason for the acoustic eigenfrequency to be conserved. Yet, it still falls well in-between the two limiting values determined in §2.3 (see also Table 3): $44 < f_a < 99$ Hz. The acoustic and hydrodynamic

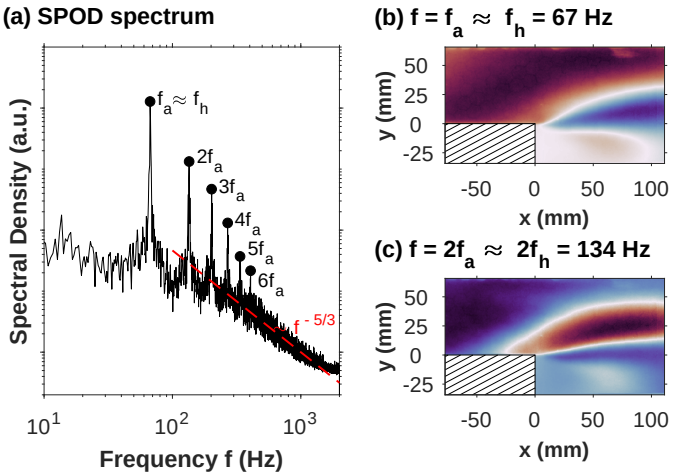

Figure 9: **(a)** SPOD spectrum of the recordings for the Unstable Case. **(b)** SPOD shape of the $f = 67$-Hz mode. **(c)** SPOD shape of the $f = 134$-Hz mode. For each mode, an animation of the shape is provided in the Supplementary materials S10 and S11.

modes now appear to be fully coupled. This manifests by the presence of a single peak at $f_a \approx f_h$, which results from the shift of both frequencies to a common value. Indeed, if we admit that this extreme coupling occurs because $f_a \approx f_h$, then we may evaluate the Strouhal number of the instability to $St_h = 0.0460$, a value within only, 6% and 10% of those obtained for the Stable and Metastable cases, respectively.

Although the outlet acoustic impedance is unknown, it is possible to determine the longitudinal profiles of the acoustic pressure $\widetilde{p}$ and velocity $\widetilde{u}$ by specifying the frequency of the longitudinal eigenmode to f_a. Figure 10 hence shows the result of such a computation. It is particularly interesting to note that the position of the step at $x = 0$ m coincides with the location of a velocity anti-node, *i.e.*, a position where the velocity is subjected to the highest amplitude of fluctuations. This point will prove to be crucial in the emergence of the flashback.

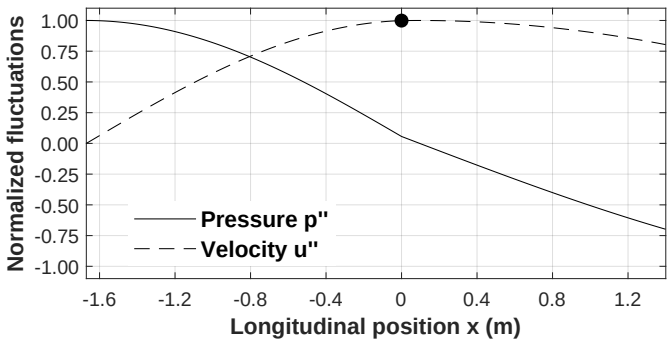

Figure 10: Profiles of the acoustic pressure and velocity normalized fluctuations in the Cfg. B for the longitudinal eigenmode at $f = f_a = 67$ Hz. Note the presence of a velocity anti-node at the location of the step (black circle).

4.4. Summary

The observations gathered so far allow us to assert that the flame motion can be explained by the coupling, or lack thereof,

between two mechanisms: *(i)* a longitudinal acoustic resonance of the ducted combustor and *(ii)* a hydrodynamic instability induced by the step. Each mechanism is characterized by a frequency: *(i)* f_a and *(ii)* f_h. The proximity between the two frequencies $\Delta f = |f_a - f_h|$ controls the intensity of the coupling. That is, as Δf decreases, the flame motion transits from a stable to an unstable behaviour. Besides, the SPOD analysis highlighted the coherent nature of the motion leading to the hydro-acoustic coupling, *i.e.*, that of a vertical flapping motion of the flame (induced by the acoustic resonance), which gets more and more amplified by the flame roll-up (corresponding to the hydrodynamic mode) as Δf decreases. We suspect that the presence of heat release in the processes induces non-linearity which manifests by a characteristic spectrum featuring peaks at the fundamental acoustic frequency and at every higher harmonics (both even and odd ones).

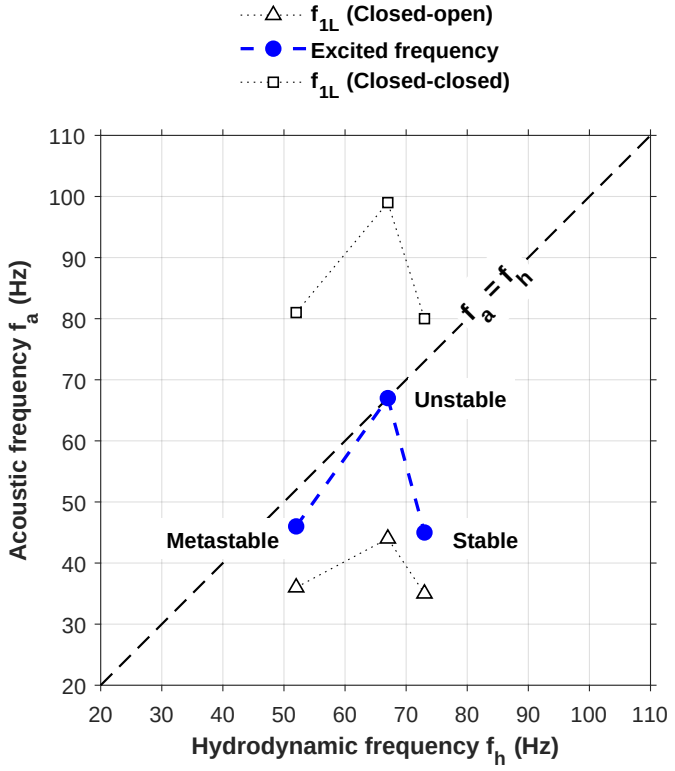

Figure 11: Positions of the studied cases in the (f_h, f_a) plane, providing, in a qualitative sense, a metering of the hydro-acoustic coupling strength. The expected frequencies for the longitudinal fundamental eigenmode considering the two-limiting models of a closed-open and a closed-closed ducts are also indicated. The closer a point is to the $f_a = f_h$-line ($\Delta f \to 0$), the stronger the hydro-acoustic coupling is.

The value of Δf is specified by the operating conditions. That is, the hydrodynamic frequency f_h is, to the first-order, controlled by the average flow velocity u_0, whereas the acoustic frequency f_a is controlled by the temperature T_0 of the inlet flow and the length of the duct $L = L_{in} + L_c$. Figure 11 shows how the different cases locate in the (f_h, f_a) plane. The expected frequencies for the longitudinal fundamental eigenmode, considering the two-limiting models of a closed-open and a closed-closed ducts, are also indicated. For the Unstable Case, the proximity $f_a \approx f_h$ triggers the hydro-acoustic coupling. This implies large amplitude fluctuations of the flow velocity up to the point that it drops below the flame speed, even more so because the flame locates itself in the vicinity of a velocity antinode. This point is quantitatively examined in the following section.

5. Flame position discussion

In order to analyse how the flame positions itself relative to the incoming flow, we use the mean position of the flame front measured in Fig. 6. For the Stable Case, we measure that the flame front is oriented at a mean angle $\alpha_0 \approx 11°$ with respect to the longitudinal direction. Using a geometrical analogy with a Bunsen flame, it is possible to evaluate the flame speed s_f according to:

$$s_f = u_0 \sin(\alpha_0) \tag{7}$$

That is, the component of the flow velocity normal to the flame front is equal to the flame speed. We obtain $s_f \approx 11$ m/s.

Lieuwen [27] proposed the triple decomposition concept to have the flow velocity $u(t)$ written as:

$$u(t) = u_0 + \widetilde{u}(t) + u'(t) \tag{8}$$

, where $\widetilde{u}(t)$ and $u'(t)$ represents the coherent and turbulent fluctuations, respectively. Now suppose that $\widetilde{u}$ is modulated by a sine wave of frequency f_a and phase Φ (*i.e.*, only the acoustic fluctuations are considered), and that u' follows a normal distribution. That is:

$$\begin{cases} \widetilde{u}(t) = \sqrt{2}\widetilde{u}_{rms} \sin(2\pi f_a t + \Phi) \\ u'(t) = \mathcal{N}(0, u'_{rms}) \end{cases} \tag{9}$$

, where $\mathcal{N}(0, u'_{rms})$ represents a normally distributed random variable with mean value 0 and standard deviation u'_{rms}. Filtering out the turbulent velocity fluctuations, it is possible to build a kinematic model for the angle α of the flame front:

$$\begin{cases} u(t) = u_0 + \widetilde{u}(t) \\ \alpha(t) = \sin^{-1}\left(\dfrac{s_f}{u(t)}\right) \end{cases} \tag{10}$$

We consider that the acoustic velocity amplitude does not significantly change at the vicinity of the step. By means of the model (Eq. (10)) and through a qualitative comparison with the flame motion recordings (see Fig. 5(a)), it is possible to approximate the rms of the acoustic velocity fluctuations. We find $\widetilde{u}_{rms} \approx 7$ m/s. The PIV measurements reported in [2–4] for the Stable Case indicates an overall rms value of $u_{rms} = 10$ m/s. Hence, the rms of the turbulent fluctuating velocity is evaluated to $u'_{rms} = \sqrt{u_{rms}^2 - \widetilde{u}_{rms}^2} \approx 7$ m/s. Injecting this value into the formulation [62, 63] for the turbulent flame speed:

$$s_t = s_L \sqrt{\frac{u' \ell_t}{s_L \delta_\ell^0}} \tag{11}$$

we obtain $s_f = s_t \approx 11$ m/s, *i.e.,* the same value of s_f obtained from the evaluation of the mean flame front position (see Eq. (7)).

For the Metastable Case, the flame front is oriented at a mean angle $\alpha_0 \approx 15°$. According to Eq. (7), this yields a flame speed $s_f \approx 11$ m/s, the same value obtained for the Stable Case, which indicates that the incoming flow turbulent conditions are similar between the two cases.

For the Unstable Case, the very concept of a flame angle no longer applies, since the flame front never stabilizes itself. Nevertheless, because of the hydro-acoustic coupling occurring for this case, it is presumed that the flashback of the flame results from the velocity of the flow falling below the flame speed. As a matter of fact, we have determined in §4.3 that a velocity antinode (*i.e.*, with the largest fluctuations) is present at the position of the step. This argument is quantitatively analysed in the following.

On the one hand, we suppose that the turbulent fluctuating velocity is equal to that estimated for the Stable Case, *i.e.,* $u'_{rms} \approx 7$ m/s. As such, the flame speed is evaluated according to Eq. (11) to $s_f = s_t \approx 15$ m/s (recall that $s_L \approx 0.5$ m/s for the Stable and Metastable cases, and $s_L \approx 0.8$ m/s for the Unstable Case, see §2.2). On the other hand, considering the PIV-returned rms value of the overall velocity fluctuations reported in [2–4]: $u_{rms} = 45$ m/s, we evaluate the hydro-acoustic velocity fluctuations to $\widetilde{u}_{rms} = \sqrt{u_{rms}^2 - {u'_{rms}}^2} \approx 44$ m/s. It is now tempting to evaluate the relative period τ_{fb} of the flashback within one oscillation period $\tau_a = 1/f_a$. We define it as the time period during which the flow velocity falls below the flame speed. In statistical terms, this is evaluated as:

$$\frac{\tau_{fb}}{\tau_a} = \int_{-\infty}^{s_f} \mathrm{pdf}(u)\, du \qquad (12)$$

, where pdf(u) is the Probability Density Function (PDF) of u. Figure 12(a) shows the oscillations of $u(t)$ modeled according to Eqs. (8) and (9). Fig. 12(b) provides with the corresponding PDF of u. Numerical integration of Eq. (12) yields

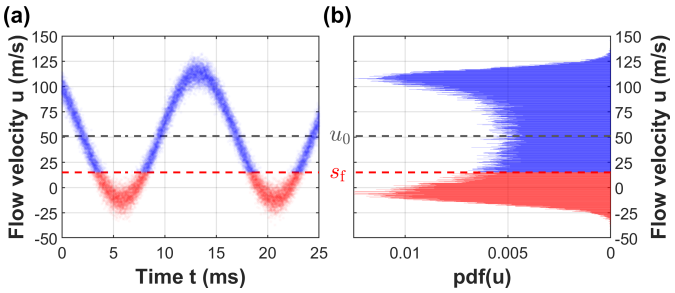

Figure 12: **(a)** Time fluctuations of $u(t)$ for the Unstable Case modeled according to Eqs. (8) and (9). **(b)** Probability distribution of u. The red color indicates the flashback condition, *i.e.*, $u < s_f$.

$\tau_{fb}/\tau_a = 0.307$. This result is well confirmed by the experimental observation.

To illustrate this point, Figure 13 displays a selection of snapshots selected at regular intervals within one oscillation period $\tau_a \approx 15$ ms. This constitutes one sample of a flashback cycle out of the 205 recorded. In addition, Figure 13 provides, for comparison, the evolution of the velocity u of the flow modeled according to Eqs. (8) and (9). It can be noted that the flashback

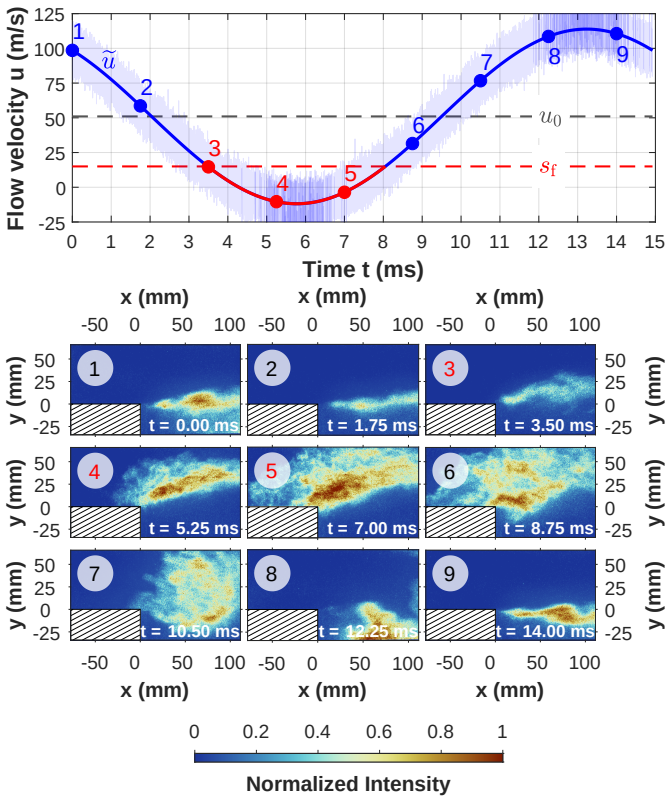

Figure 13: Illustration of the flashback cycle within one oscillation period. The top graph allows for comparison between the velocity u of the flow modeled according to Eqs. (8) and (9), and the assumed value for the flame speed $s_f = 15$ m/s. The solid line represents the fluctuations $\widetilde{u}$ imposed by the hydro-acoustic coupling, over which the stochastic, *i.e.*, turbulent fluctuations are added to form the light-blue curve.

motion incepts at the time $t \approx 3.5$ ms, which corresponds to the time at which $\widetilde{u}$ drops below s_f. The flashback motion ends at $t \approx 8.25$ ms and corresponds to the instant around which the bulk OH* intensity stops from counter-flowing (see the video in the Supplementary material S3). Again, this is in-line with the time when $\widetilde{u}$ exceeds s_f. The relative flashback period is therefore experimentally estimated to $\tau_{fb}/\tau_a = 0.318$, which is very close to the value obtained from Eq. (12). In fact, by analyzing the complete set of flashback cycles recorded, we converged to a mean value of $\tau_{fb}/\tau_a = 0.305$ with a standard deviation of 0.04. This results is quite remarkable considering the underlying hypotheses that led to the evaluation of τ_{fb}/τ_a. One of which is the sine wave form presumed for modelling $\widetilde{u}$. Besides, the existence of a threshold, when $u < s_f$, induces an abrupt shift in the dynamics of the system, a manifestation of a strong non-linear behaviour, which could not merely reduce to a sine wave description. Indeed, in [2, 4], the signal recorded by the pressure transducer, located on the top wall and at an axial position $x = 1.5$ cm from the step, follows a non-linear periodical pattern of which the progressive growth and decay phases are disrupted by a sudden rise and drop, respectively. Nonetheless, we

believe that the sine-wave assumption did not introduce significant errors because the system dynamics, although non-linear in nature, still remains periodical.

Besides, time-synchronization with the OH* chemiluminescence recording (deemed as an integration in the z-direction of the heat-release) appears to indicate that the local Rayleigh criterion is negative, that is the period where $\widetilde{p} > 0$ corresponds to negative fluctuations of the local heat-release. This suggests that, locally, the pressure and heat release are in phase opposition. However, this does not mean that the Rayleigh criterion is negative everywhere, *i.e.,* a thermo-acoustic coupling could still be at play further downstream.

It is well known that flashback in ducted combustors can develop in near-wall regions [9, 16], especially in the boundary layer above the step (see the $t = 5.25$ ms snapshot on Fig. 13). However, we believe the flame to first propagate towards this location due to the condition $u < s_f$ rather than being initiated inside of it.

As the velocity of the flow continues to rise, the flame is pushed downstream because $u > s_f$ and stabilizes away from the step for a brief period of time. Again, the time at which the velocity reaches its maximum, *i.e.*, $t \approx 13$ ms, coincides with the time when the flame reaches the most downstream position in Fig. 13.

It is important to note that these observations complete the interpretations established in [2–4]. The flashback motion was, at the time, interpreted as resulting from a flow reversal. We interpret it as originating from the velocity of the flow falling below that of the flame. Actually, had the flow velocity stayed positive, the flashback could well have been observed. As a matter of fact, the integration of the PDF from $-\infty$ to 0 (as opposed to integrating from $-\infty$ to s_f) yields $\tau_{fb}/\tau_a \approx 0.18$, which is further away from the value deduced from the experiments.

6. Characterization of the limit-cycle attractor

It is interesting to note the emergence of some sort of order when the hydro-acoustic coupling is at play. In order to describe this, we elaborate on a time-series analysis of the system dynamics.

6.1. Choice of the state variable

We begin by defining a state variable for the system susceptible of capturing the motion dynamics. Natural candidates for this would be the pressure or velocity fluctuations. However, we want to limit our analysis to the imaging data, in making a point that they are efficient at capturing the dynamics of such a non-linear system. Consequently, possible candidates, would be the local or space averaged intensities. Other kinds of candidates would be geometrical parameters describing the flame kinematics. It is tempting to use the polar coordinate to describe the position of the flame, since the flashback motion is somehow analogue to that of a pendulum, even-though the tip of the step does not constitute an absolute center of rotation for the flame. In practice, we use the angle θ measuring the angular position (relative to the horizontal direction) of the flame intensity centroid (intensity-weighted center of mass) with an origin placed at the tip of the step. Figure 14 sketches the definition of θ from the computed location of the flame intensity centroid (labeled C).

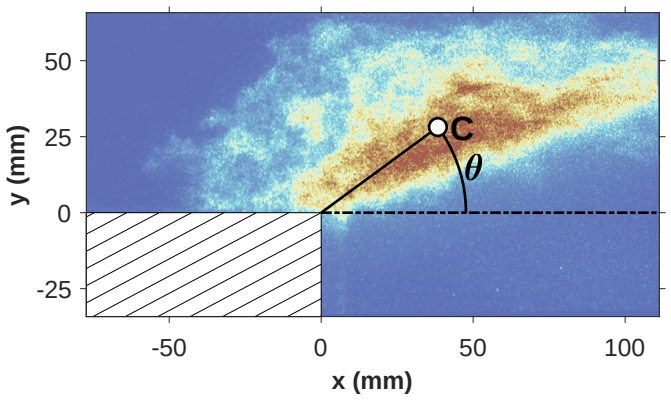

Figure 14: Definition of the angle θ from the computed location C of the flame intensity centroid.

6.2. Time-series analysis

Figure 15 shows the variation of θ for the Unstable Case. We recognize the strong periodical nature of the oscillation, but with the non sine-wave form imposed by the presence of the velocity threshold in the dynamics. Note that the variation of θ are framed such that $-15° < \theta < 130°$. The upper bound is, in

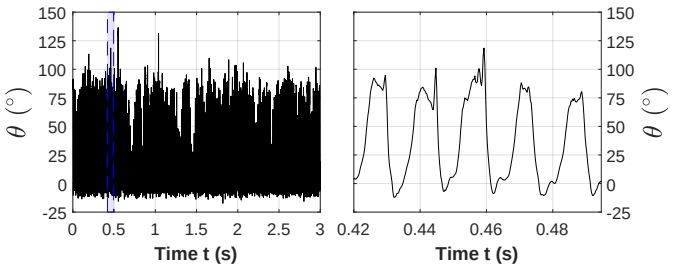

Figure 15: Unstable Case: time series of the angle θ. The right graph shows a zoom-in of the fluctuations within the blue-shaded area displayed on the left graph.

all likelihood, actually higher, because the flame may, at times, propagate upstream of the zone covered by the visualization window. The motion amplitude varies from cycle to cycle, of which the modulation is not quantitatively understood, hence presumed of stochastic nature. Notice the occasional bursts of θ as one can be observed around $t = 0.45$ s in the zoomed-in graph of Fig. 15. By examining in details the images sequence around that time (see Fig. 16), we observe the creation of a second flame front in the top-left corner of the visualization zone ($x = -50$ mm, $y = 65$ mm), almost at the same time as the flashback incepts. We suspect that the second flame is an autoignition front consecutive of *(i)* the presence of a local hot spot at the top wall surface, and *(ii)* the temporal low-velocity found in the region, even more so in the boundary layer, thereby favoring its growth. The explanation for the presence of a hot spot at this location is two-fold. On the one hand, it may come from the

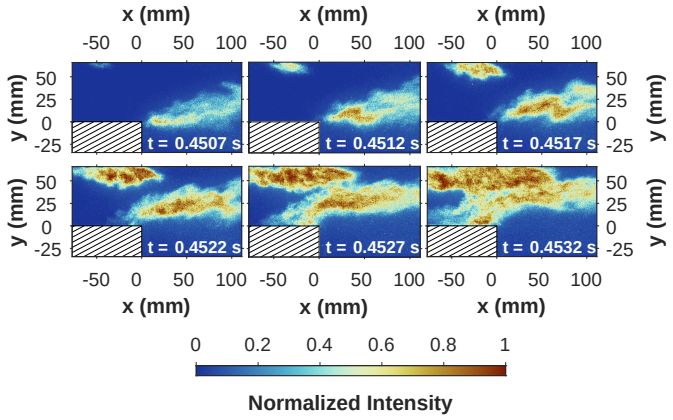

Figure 16: Sequence of images corresponding to the double burst in θ observed around $t = 0.45$ s in Fig. 15 (right). Note the creation and growth of an autoignition front originating from the top wall. A videos showing this peculiar flashback cycle is provided in the Supplementary material 12.

non-nominal increase of the wall temperature resulting from the previous flashback cycles. On the other hand, it may be caused by the localized hot spots impaired by the non-uniform cooling of the combustor walls, in particular at the junction between the top uncooled quartz window (for the PLIF and PIV laser sheets, not reported in the present paper) and the water-cooled wall onto which the window is mounted. As for the intermittency of what could be deemed as an extreme event, we could only speculate at this stage that it is stochastic. It appears that in this peculiar cycle, the flame propagates much farther upstream, and explains why the amplitude of θ is, in this cycle, higher than in the others. The fact that the visualization windows does not cover the whole spatial extent of the dynamics induces non-physical local fluctuations of θ. During the period of time when the flame front propagates upstream of the visualization window, the angle of rotation θ is somehow ill-characterized: the flame intensity centroid is interpreted as lagging downstream in the burnt gases whereas, it is in reality in the blind upstream portion of the duct. When the flame is pushed forward, *i.e.*, the flow velocity increases, a very brief second burst is observed as a consequence of the flame front re-appearing in the visualization zone. In summary, the two apparent peaks observed in the time-series of Fig. 15 should really be interpreted as a single one. The generation of autoignition fronts is a stochastic process, which is a characteristic trait often encountered in forced ignition or autoignition of turbulent reactive flows. The event is actually quite rare as it is only observed six times out of a total of 205 flashback cycles recorded, *i.e.*, with an occurrence probability of about 3%.

6.3. Characterization of the limit-cycle attractor

We propose to characterize the nature of the flashback motion dynamics. To do so, the phase space reconstruction for the chosen state variable, θ, is performed by means of delay-coordinated embedding [64]. The embedding parameters, namely the time-lag τ and the embedding dimension m, are set according to standard practices. The time-lag τ is set as the time corresponding to the first minimum of the average mutual information [65], of which Figure 17(a) shows the variation with τ. The first minimum is thus found at $\tau = 4$ ms. As for the embedding dimension m, we use the False Nearest Neighbor (FNN) algorithm proposed by Kennel *et al.* [66]. As shown in Fig. 17(b), an $m = 3$-dimensions embedding is convincingly sufficient to reconstruct the dynamics since the fraction of FNN drops below 3% after three embeddings. Figure 18

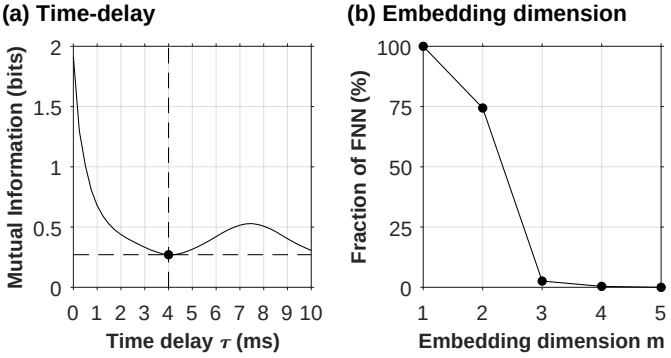

Figure 17: Determination of the embedding parameters for the phase reconstruction based on the chosen state variable θ. **(a)** Average Mutual information for the time-delay τ determination. **(b)** Fraction of False Nearest Neighbors (FNN) for the determination of the embedding dimension m.

finally shows the reconstructed trajectory in the phase space. The trajectory is clearly ordered with its shape threading around a closed orbit, *i.e.*, that of a limit-cycle attractor. It much differs from the circular orbit characteristic of a harmonic oscillator, and the spiralling-in or out orbits characteristic of positively (stable) and negatively (unstable) damped harmonic oscillators. The trajectory does not overlap, which indicates that the $m = 3$-dimensions embedding is appropriate. The somehow large thickness of the limit-cycle trajectory, which departs from a two-dimension object, *i.e.*, a curve, is due to *(i)* the error induced by the rather crude estimation of θ, which is intrinsically bounded as a consequence of the visualization zone limitation and *(ii)* the stochastic modulation of the flashback motion amplitude.

7. Conclusions

This work brings new insights into the comprehension of the flashback dynamics of a high Reynolds-number ducted premixed flame establishing around a backward-facing step, a situation which has direct implication in the design of safer and reliable propulsive or energy conversion systems. We have resumed the analysis of an experimental database collected at ONERA some years ago and have based our works on the spectral examination of the high-speed recordings acquired at that time.

The 1D acoustic analysis combined to the SPOD technique allowed us to decompose the flame motion into two main components: *(i)* a vertical flapping motion induced by a longitudinal acoustic resonance of the ducted combustor, and *(ii)* a hydrodynamic instability related to the flame roll-up motion in the recirculation bubble trailing the step. The latter appears to be

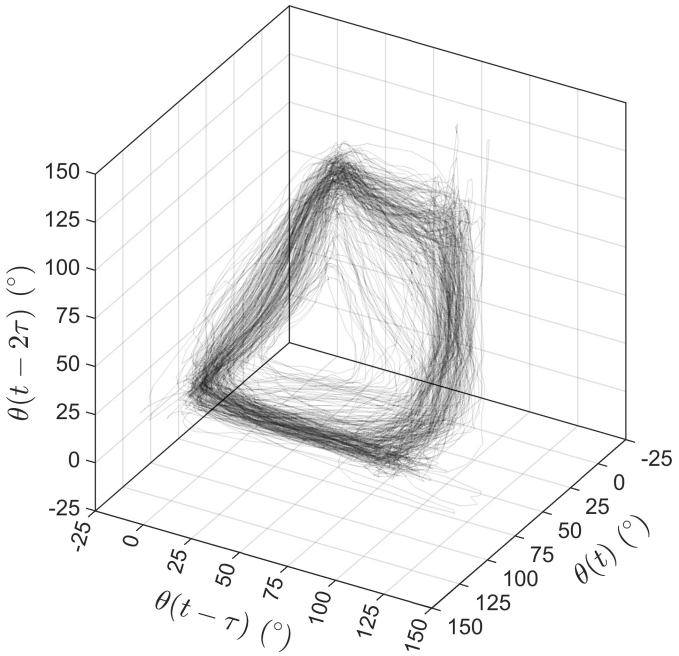

Figure 18: Reconstructed phase portrait for the angle θ representing the rotational motion of the flame intensity centroid.

self-similar and as such is characterized with a Strouhal Number, based on the step height h_s and bulk flow velocity u_0, to a value $\mathrm{St_h} = f_h h_s/u_0 = 0.044 \pm 5\%$. When the characteristic frequencies associated to these two coexisting mechanisms are far apart, the flame is relatively stable, in that its position is quite steady. As the frequencies approaches each other, a coupling begins to develop: the amplitude of the flame flapping motion significantly increases with moderate excursion of the flame front upstream of the step. When the two frequencies coincide, the coupling is fully established. This prompts the emergence of the flashback since the fluctuations of the hydroacoustically modulated flow velocity are so large that the flow velocity temporally drops below the flame speed. The presence of a velocity anti-node close to the step location amplifies the level of fluctuations.

Phase space reconstruction of the flame rotation, which defines a state variable for the kinematic characterization of the system, reveals that the dynamics is locked to a stable limit-cycle. A certain stochasticity exists in the process, according to which a concomitant second flame front, seemingly that of an autoignition front, onsets and grows in the vicinity of the top wall boundary layer, at the moment where the main front begins to propagate upstream. The autoignition front onsets without any regularity and is observed with a 3% occurrence probability. We suspect that the intermittent autoignition originates from the presence of a localized hot spot on the combustion chamber top wall, which is non-uniformly cooled.

Although a satisfactory flashback scenario relying on the coupling between an acoustic mode and a hydrodynamic mode has been proposed, the existence of a thermo-acoustic coupling, or lack thereof could not be ascertained. Besides, the study of the flame response to acoustic modulation could constitute another research focus. Accounting for the flame response contribution into the 1D acoustic analysis could enable a clearer representation of the natural modes shapes, frequencies, and growth rates. Furthermore, additional works are required to extract the underlying governing equation describing the flashback limit-cycle and the mechanism responsible for the cycle-to-cycle variation of the motion amplitude.

Another possible extension of this work could be the study of the transient evolutions leading from the Stable Case dynamics to the Unstable dynamics in the same combustor geometry. In other words, this means describing the bifurcation dynamics of the system. Such transient evolutions could be achieved by ramping-up or down the equivalence ratio ϕ, the inlet temperature T_0 or the combustor pressure P.

This study is part of a larger framework focused on the contribution of the flame motions in destabilizing a flow [67]. Further exploration of the underlying mechanisms should be performed in future works, owing to ongoing numerical simulations [19].

Acknowledgements

This work was funded by ONERA, the French Aerospace Lab. We gratefully acknowledge Ajmal K. Mohamed, Joel Dupays, Laurent Jacquin, Philippe Villedieu, Jérôme Anthoine and Olivier Dessornes for their continuous support in the research of combustion dynamics.

References

[1] V. Sabelnikov, F. Grisch, M. Orain, Instabilities and structure of turbulent premixed flame in a lean stepped combustor, 17th International Society for Air Breathing Engines (ISABE) Conference (2005).

[2] V. Sabelnikov, C. Brossard, M. Orain, F. Grisch, M. Barat, A. Ristori, P. Gicquel, Thermo-acoustic instabilities in a backward-facing step stabilized lean-premixed flame in high turbulence flow, 14th International Symposium on Applications of Laser Techniques to Fluid Mechanics (2008).

[3] C. Brossard, V. Sabelnikov, M. Orain, F. Grisch, M. Barat, A. Ristori, P. Gicquel, Étude expérimentale des instabilités thermo-acoustiques d'une flamme turbulente prémélangée, Congrès Francophone de Techniques Laser (2008).

[4] V. Sabelnikov, C. Brossard, M. Orain, F. Grisch, M. Barat, A. Ristori, P. Gicquel, Visualization study of thermo-acoustic instabilities in a backward-facing step stabilized lean-premixed flame in high turbulence flow, 10th Conference (International) on Fluid Control, Measurements, and Visualization (2009).

[5] A. Towne, O. T. Schmidt, T. Colonius, Spectral proper orthogonal decomposition and its relationship to dynamic mode decomposition and resolvent analysis, J. Fluid Mech. 847 (2018) 821–867.

[6] T. Lieuwen, V. McDonell, D. Santavicca, T. Sattelmayer, Burner development and operability issues associated with steady flowing syngas fired combustors, Combust. Sci. Technol. 180 (2008) 1169–1192.

[7] T. Lieuwen, V. McDonell, E. Petersen, D. Santavicca, Fuel flexibility influences on premixed combustor blowout, flashback, autoignition, and stability, J. Eng. Gas Turbines Power 130 (2008).

[8] S. Plee, A. Mellor, Review of flashback reported in prevaporizing/premixing combustors, Combust. Flame 32 (1978) 193–203.

[9] A. Kalantari, V. McDonell, Boundary layer flashback of non-swirling premixed flames: Mechanisms, fundamental research, and recent advances, Prog. Energ. Combust. 61 (2017) 249–292.

[10] R. J. Kee, M. E. Coltrin, P. Glarborg, H. Zhu, Chemically Reacting Flow, John Wiley & Sons, Hoboke, N.J., U.S., 2017.

[11] P.-H. Renard, D. Thevenin, J.-C. Rolon, S. Candel, Dynamics of flame/vortex interactions, Prog. Energ. Combust. 26 (2000) 225–282.

[12] K. S. Kedia, A. F. Ghoniem, The anchoring mechanism of a bluff-body stabilized laminar premixed flame, Combust. Flame 161 (2014) 2327–2339.

[13] M. Konle, F. Kiesewetter, T. Sattelmayer, Simultaneous high repetition rate PIV–LIF-measurements of CIVB driven flashback, Exp. Fluids 44 (2008) 529–538.

[14] V. Kurdyumov, E. Fernandez, A. Linan, Flame flashback and propagation of premixed flames near a wall, Proc. Combust. Inst. 28 (2000) 1883–1889.

[15] V. Hoferichter, C. Hirsch, T. Sattelmayer, Prediction of confined flame flashback limits using boundary layer separation theory, J. Eng. Gas Turb. Power 139 (2017).

[16] D. Thibaut, S. Candel, Numerical study of unsteady turbulent premixed combustion: Application to flashback simulation, Combust. Flame 113 (1998) 53–65.

[17] Y. Sommerer, D. Galley, T. Poinsot, S. Ducruix, F. Lacas, D. Veynante, Large eddy simulation and experimental study of flashback and blow-off in a lean partially premixed swirled burner, J. Turb. 5 (2004) N37.

[18] D. Ebi, N. T. Clemens, Experimental investigation of upstream flame propagation during boundary layer flashback of swirl flames, Combust. Flame 168 (2016) 39–52.

[19] J.-M. Klein, A. Genot, A. Vincent-Randonnier, A. Mura, Combustion thermoacoustics: on the relevance of some stability criteria, 9th European Conference For Aeronautics And Space Sciences EUCASS-3AF (2022).

[20] Y. Wu, V. Modica, X. Yu, F. Grisch, Experimental Investigation of Laminar Flame Speed Measurement for Kerosene Fuels: Jet A-1, Surrogate Fuel, and Its Pure Components, Energ. Fuels 32 (2018) 2332–2343.

[21] N. Donohoe, A. Heufer, W. K. Metcalfe, H. J. Curran, M. L. Davis, O. Mathieu, D. Plichta, A. Morones, E. L. Petersen, F. Güthe, Ignition delay times, laminar flame speeds, and mechanism validation for natural gas/hydrogen blends at elevated pressures, Combust. Flame 161 (2014) 1432–1443.

[22] S. Hemchandra, S. Shanbhogue, S. Hong, A. F. Ghoniem, Role of hydrodynamic shear layer stability in driving combustion instability in a premixed propane-air backward-facing step combustor, Phys. Rev. Fluids 3 (2018) 063201.

[23] F. Nicoud, L. Benoit, C. Sensiau, T. Poinsot, Acoustic modes in combustors with complex impedances and multidimensional active flames, AIAA J. 45 (2007) 426–441.

[24] P. G. Drazin, W. H. Reid, Hydrodynamic stability, Cambridge University Press, Cambridge, U.K., 2004.

[25] B. Emerson, J. O'Connor, M. Juniper, T. Lieuwen, Density ratio effects on reacting bluff-body flow field characteristics, J. Fluid Mech. 706 (2012) 219–250.

[26] B. Emerson, T. Lieuwen, Dynamics of harmonically excited, reacting bluff body wakes near the global hydrodynamic stability boundary, J. Fluid Mech. 779 (2015) 716–750.

[27] T. C. Lieuwen, Unsteady combustor physics, Cambridge University Press, Cambridge, U.K., 2021.

[28] K. Manoharan, S. Hemchandra, Absolute/convective instability transition in a backward facing step combustor: Fundamental mechanism and influence of density gradient, J. Eng. Gas Turb. Power 137 (2015).

[29] K. I. Matveev, F. Culick, A model for combustion instability involving vortex shedding, Combust. Sci. Technol. 175 (2003) 1059–1083.

[30] V. Nair, R. Sujith, A reduced-order model for the onset of combustion instability: physical mechanisms for intermittency and precursors, Proc. Combust. Inst. 35 (2015) 3193–3200.

[31] A. F. Ghoniem, A. Annaswamy, D. Wee, T. Yi, S. Park, Shear flow-driven combustion instability: Evidence, simulation, and modeling, Proc. Combust. Inst. 29 (2002) 53–60.

[32] K.-B. Chun, H. J. Sung, Control of turbulent separated flow over a backward-facing step by local forcing, Exp. Fluids 21 (1996) 417–426.

[33] D. Wee, S. Park, T. Yi, A. Annaswamy, A. Ghoniem, Reduced order modeling of reacting shear flow, 40th AIAA Aerospace Sciences Meeting & Exhibit (2002) , paper 478.

[34] H. N. Najm, A. F. Ghoniem, Coupling between vorticity and pressure oscillations in combustion instability, J. Propul. Power 10 (1994) 769–776.

[35] D. M. Driver, H. L. Seegmiller, J. G. Marvin, Time-dependent behavior of a reattaching shear layer, AIAA J. 25 (1987) 914–919.

[36] M. Hasan, The flow over a backward-facing step under controlled perturbation: laminar separation, J. Fluid Mech. 238 (1992) 73–96.

[37] N. Benard, P. Sujar-Garrido, J.-P. Bonnet, E. Moreau, Control of the coherent structure dynamics downstream of a backward facing step by DBD plasma actuator, Int. J. Heat Fluid Flow 61 (2016) 158–173.

[38] C.-M. Ho, L.-S. Huang, Subharmonics and vortex merging in mixing layers, J. Fluid Mech. 119 (1982) 443–473.

[39] P. Spazzini, G. Iuso, M. Onorato, N. Zurlo, G. Di Cicca, Unsteady behavior of back-facing step flow, Exp. Fluids 30 (2001) 551–561.

[40] V. Statnikov, I. Bolgar, S. Scharnowski, M. Meinke, C. Kähler, W. Schröder, Analysis of characteristic wake flow modes on a generic transonic backward-facing step configuration, Eur. J. Mech. B-Fluid 59 (2016) 124–134.

[41] X. Ma, A. Schröder, Analysis of flapping motion of reattaching shear layer behind a two-dimensional backward-facing step, Phys. Fluids 29 (2017) 115104.

[42] I. Bolgar, S. Scharnowski, C. J. Kähler, The effect of the Mach number on a turbulent backward-facing step flow, Flow Turbul. Combust. 101 (2018) 653–680.

[43] J. O. Keller, J. Daily, The effects of highly exothermic chemical reaction on a two-dimensional mixing layer, AIAA J. 23 (12) (1985) 1937–1945.

[44] H. M. Altay, R. L. Speth, D. E. Hudgins, A. F. Ghoniem, Flame–vortex interaction driven combustion dynamics in a backward-facing step combustor, Combust. Flame 156 (2009) 1111–1125.

[45] S. Hong, S. J. Shanbhogue, R. L. Speth, A. F. Ghoniem, On the phase between pressure and heat release fluctuations for propane/hydrogen flames and its role in mode transitions, Combust. Flame 160 (2013) 2827–2842.

[46] B. Nagarajan, N. Baraiya, S. Chakravarthy, Effect of inlet flow turbulence on the combustion instability in a premixed backward-facing step combustor, Proc. Combust. Inst. 37 (2019) 5189–5196.

[47] W. L. Roberts, J. F. Driscoll, A laminar vortex interacting with a premixed flame: measured formation of pockets of reactants, Combust. Flame 87 (1991) 245–256.

[48] A. P. Dowling, A kinematic model of a ducted flame, J. Fluid Mech. 394 (1999) 51–72.

[49] F. Culick, T. Rogers, The response of normal shocks in diffusers, AIAA J. 21 (1983) 1382–1390.

[50] E. Bekaert, A. Genot, T. Le Pichon, T. Schuller, Low-order models for acoustic modes in a ramjet combustor with inlet shock train, 9th European Conference For Aeronautics And Space Sciences EUCASS-3AF (2022).

[51] R. Bounaceur, P.-A. Glaude, B. Sirjean, R. Fournet, P. Montagne, M. Vierling, M. Molière, Prediction of Auto-Ignition Temperatures and Delays for Gas Turbine Applications, J. Eng. Gas Turb. Power 138 (2016) 021505.

[52] J. O. Keller, L. Vaneveld, D. Korschelt, G. L. Hubbard, A. F. Ghoniem, J. W. Daily, A. K. Oppenheim, Mechanism of instabilities in turbulent combustion leading to flashback, AIAA J. 20 (1982) 254–262.

[53] H. M. Altay, R. L. Speth, D. E. Hudgins, A. F. Ghoniem, The impact of equivalence ratio oscillations on combustion dynamics in a backward-facing step combustor, Combust. Flame 156 (2009) 2106–2116.

[54] M. Akram, P. Saxena, S. Kumar, Laminar Burning Velocity of Methane–Air Mixtures at Elevated Temperatures, Energ. Fuels 27 (6) (2013) 3460–3466.

[55] R. Borghi, On the structure and morphology of turbulent premixed flames, Recent advances in the Aerospace Sciences (1985) 117–138.

[56] M. Meissner, Effect of Cross-Sectional Area Discontinuities in Closed Hard-Walled Ducts on Frequency of Longitudinal Modes, Arch. Acoust. 35 (Jan. 2010).

[57] K. Taira, S. L. Brunton, S. T. M. Dawson, C. W. Rowley, T. Colonius, B. J. McKeon, O. T. Schmidt, S. Gordeyev, V. Theofilis, L. S. Ukeiley, Modal Analysis of Fluid Flows: An Overview, AIAA J. 55 (2017) 4013–4041.

[58] S. Boulal, N. Fdida, L. Matuszewski, L. Vingert, M. Martin-Benito, Flame dynamics of a subscale rocket combustor operating with gaseous methane and gaseous, subcritical or transcritical oxygen, Combust. Flame 242 (2022) 112179.

[59] O. T. Schmidt, T. Colonius, Guide to Spectral Proper Orthogonal Decomposition, AIAA J. 58 (2020) 1023–1033.

[60] R. H. Kraichnan, Inertial Ranges in Two-Dimensional Turbulence, Phys. Fluids 10 (1967) 1417–1423.

[61] A. N. Kolmogorov, The local structure of turbulence in incompressible viscous fluid for very large reynolds number, Dokl. Akad. Nauk. SSSR 30 (1941) 301–303.

[62] G. Damköhler, The Effect of Turbulence on the Flame Velocity in Gas Mixtures, Zeitschrift für Elektrochemie und Angewandte Physikalische Chemie 46 (1947).
[63] N. Peters, Turbulent combustion, Cambridge University Press, Cambridge, U.K., 2000.
[64] H. Kantz, T. Schreiber, Nonlinear Time Series Analysis, 2nd Edition, Cambridge University Press, Cambridge, U.K., 2003.
[65] A. M. Fraser, H. L. Swinney, Independent coordinates for strange attractors from mutual information, Phys. Rev. A 33 (1986) 1134–1140.
[66] M. B. Kennel, R. Brown, H. D. Abarbanel, Determining embedding dimension for phase-space reconstruction using a geometrical construction, Phys. Rev. A 45 (1992) 3403–3411.
[67] J.-M. Klein, A. Gandilhon-Gounelle, A. Vincent-Randonnier, A. Genot, A. Mura, On the invariance of flame-motion-induced variations of the generalized disturbance energy, Combust. Flame 251 (2023) 112711.